

NOTICE

This report was prepared to document work sponsored by the United States Government. Neither the United States nor its agent, the United States Department of Energy, nor any Federal employees, nor any of their contractors, subcontractors or their employees, makes any warranty, express or implied, or assumes any legal liability or responsibility for the accuracy, completeness, or usefulness of any information, apparatus, product or process disclosed, or represents that its use would not infringe privately owned rights.

DOE/NASA/2593-79/7
NASA TM-79205

ANALYSIS OF THE RESPONSE
OF A THERMAL BARRIER
COATING TO SODIUM-
AND VANADIUM-DOPED
COMBUSTION GASES

Robert A. Miller
National Aeronautics and Space Administration
Lewis Research Center
Cleveland, Ohio 44135

Prepared for
U. S. DEPARTMENT OF ENERGY
Energy Technology
Fossil Fuel Utilization Division
Washington, D. C. 20545
Under Interagency Agreement EF-77-A-01-2593

Eighth Midwest High Temperature
Chemistry Conference
Milwaukee, Wisconsin, June 4-6, 1979

*N80-10344**

ANALYSIS OF THE RESPONSE OF A THERMAL BARRIER
COATING TO SODIUM AND VANADIUM-DOPED COMBUSTION GASES

by Robert A. Miller
National Aeronautics and Space Administration
Lewis Research Center
Cleveland, Ohio 44135

SUMMARY

Ceramic thermal barrier coatings are expected to play an important role in the future for surface protection of gas turbine components. These coatings generally consist of an outer insulating ceramic oxide layer and an inner oxidation resistant metallic bond coating. They are currently being developed for use in the clean environment of an aircraft gas turbine. Industrial/utility types of gas turbines and, under certain conditions, aircraft turbines may also be exposed to "dirty" environments. In these cases aggressive compounds such as sodium sulfate, vanadium oxide, or sodium vanadate may condense on turbine components. Thermal barrier coatings used in dirty environments must be able to protect the underlying substrate while being resistant to degradation themselves. Tests showed that an early thermal barrier coating system, ZrO₂-12 w/o Y₂O₃/NiCrAlY, failed rapidly in the presence of such contaminants.

The conditions which lead to spalling of the coatings are analyzed. Five previously conducted experiments are discussed in detail. These experiments involved coated specimens exposed to burner rig combustion gases doped with sodium and vanadium. Coating failures are explained in terms of the thermodynamic dew points and melting points of the condensates and the temperature distributions within the coatings. The location of spalled areas on the test specimens and their microstructures are explained for four of these experiments while the absence of failure is explained for the fifth.

INTRODUCTION

The environment of the hot section of a gas turbine engine is characterized by high temperatures, high pressures, high heat fluxes, and high mass fluxes. The combustion gases in the gas turbine are rich in oxygen because the fuel is burned with a great excess of air. Under certain conditions, inorganic salt contaminants are also present. Materials in the gas turbine, especially nickel-based superalloy turbine vanes and blades, are susceptible to several modes of degradation. These include chemical degradation due to oxidation and high temperature salt-induced corrosion, and mechanical degradation due to erosion, fatigue, and creep (ref. 1). These environmental effects generally become more severe as temperatures are increased. However, the effects of high temperature corrosion cease when the temperature at a given location in the turbine exceeds the dew point of the specific salt because it can no longer condense at that location.

Aircraft gas turbines currently operate at higher temperatures and pressures than other types of gas turbine engines. Future demands for increased efficiency and performance will result in still higher operating temperatures and

E-090

N80-10344

pressures. Thus, materials will have to be able to withstand even harsher conditions. The current fuels used for aircraft gas turbine operation are high purity kerosenes such as Jet A. The only significant impurity in these fuels is sulfur. Levels up to 0.3 w/o are permissible in Jet A fuel (ref. 2). Additional impurities such as sodium compounds may enter the engine through injected runway dust or sea salt aerosols. This may lead to the deposition of the highly corrosive salt sodium sulfate, Na_2SO_4 onto turbine blades and vanes.

An important non-aircraft application of gas turbine engines is in the production of electric power. These engines account for about 10% of the electric power capacity in the United States and are generally used during periods of peak demand (ref. 3). The fuels currently burned in these turbine engines are usually natural gas or various petroleum distillates. Even with the use of clean fuels, high temperature corrosion is the chief problem affecting turbine reliability. The ingestion of sea salt aerosols has been identified as a major source of these difficulties. Engines as far as 200 miles inland have been so affected (ref. 3).

In the future, gas turbine engine combined cycle systems could be competitive for base load power generation. This approach involves the recovery and use of the waste heat of the engine. The competition could be further enhanced through the use of more efficient turbine engines operating at higher temperatures and pressures. However, no loss in reliability would be acceptable. A current Department of Energy program, the High Temperature Turbine Technology program, is aimed at temperatures in the 1430° to 1650° C range. Additionally, in the future it will become necessary to burn dirtier fuels such as crude or residual fuel oil. Impurities found in these dirtier fuels may include sodium (Na), potassium (K), vanadium (V), iron (Fe), lead (Pb), phosphorous (P), and sulfur (S). Also, minimally processed coal-derived fuels may be burned in gas turbines in the future. Trace metal levels in these coal-derived fuels are somewhat uncertain, but high temperature salt corrosion may be expected to be an even more serious future concern for non-aircraft gas turbines.

The purpose of this paper is to review past tests conducted on NASA-Lewis thermal barrier coatings in combustion gases containing corrosive compounds; to calculate the dew points of such compounds; and to begin to relate such data to coating failure.

BACKGROUND

A. Thermal Barrier Coatings for High Temperature Surface Protection

Almost all advanced engines rely on the use of coatings and air cooling (ref. 4) to protect components from environmental degradation. Although most of the coatings developed to date have been metallic (refs. 5 to 7) there is now considerable interest in ceramic coatings. These are usually called "thermal barrier coatings" because the ceramic provides insulation to air-cooled turbine components. There would be several ways to take advantage of the insulation (refs. 1 and 8). Reduced metal temperatures would translate directly to improved component reliability. Conversely if the same metal temperatures were

acceptable, performance and efficiency could be increased. This is because less cooling air would be required or because gas temperatures could be increased. An additional advantage is that fabrication costs could be reduced because less elaborate cooling schemes would be required. If ceramic coatings resistant to inorganic salt corrosion can be developed, improved component durability would result in even further benefits.

Chemical and physical attributes required for potential thermal barrier coatings include low thermal conductivity, relatively high coefficient of thermal expansion, thermodynamic stability in the gas turbine environment, and mechanical stability towards thermal cycling. Typically, thermal barrier coating systems consist of plasma-sprayed single or mixed oxide ceramics applied over plasmasprayed oxidation resistant, metallic bond coats. The ceramic layer is from 0.01 to 0.06 cm thick while the bond coat is about 0.01 cm thick. Often an intermediate layer or graded zone of mixed metal and oxide is applied to minimize differences in thermal expansion.

Numerous references to the plasma spray process are available (refs. 9 and 10). The material, usually in powder form, is fed into a high velocity plasma formed by passing a gas such as argon through an electric discharge. The residence time of the powder particles in the gas is only a few milliseconds. Still, almost any material can be melted because of high heat transfer at temperatures exceeding 10 000° C. The melted particles impact upon the substrate to produce coatings which are generally quite porous and permeable. This porosity can be expected to impart improved thermal shock resistance to ceramic coatings and increased thermal protection. At the same time pathways are provided for rapid diffusion of oxygen and inorganic salt contaminants.

B. Thermal Barrier Coatings Research at NASA-Lewis

The history of thermal barrier coatings research at NASA-Lewis has been well-documented (refs. 11 and 12). These coatings were first considered in the 1950's (refs. 13 and 14), then in the 1960's (ref. 15), and again in the early 1970's (ref. 16). The applications in these studies included surface protection of both aircraft engine and rocket engine components. In the mid-1970's Stecura and Liebert (refs. 17 to 20) developed a ZrO_2 -12 w/o Y_2O_3 /NiCrAlY coating system. Impressive test results under conditions simulating aircraft gas turbine operation were reported for this system. Due to the success of this work as well as work at other laboratories (refs. 21 to 24) zirconia-based coating systems are now being extensively evaluated for potential aircraft gas turbine applications. Recently further improvement has been demonstrated. Stecura (ref. 25) has shown that two compositions, ZrO_2 -6 w/o Y_2O_3 and ZrO_2 -8 w/o Y_2O_3 , are more durable than the original ZrO_2 -12 w/o Y_2O_3 (ref. 18). These two improved coatings are compositions which correspond to the two phase region of the ZrO_2 - Y_2O_3 phase diagram (ref. 26). In addition to the advances made in the durability of the ceramic layer, improvements were also made to the NiCrAlY bond coat. The improved performance of ZrO_2 -8 w/o Y_2O_3 is illustrated by the data presented in figure 1, which was adapted from figure 8 of reference 25. As shown in this figure, the new composition survived significantly longer at the same temperature and approximately as long

at a much higher temperature than that used to investigate ZrO₂-12 w/o Y₂O₃.

C. Dirty Fuel Tests of ZrO₂-12 w/o Y₂O₃/NiCrAlY

The early version of the NASA-Lewis coating system ZrO₂-12 w/o Y₂O₃/NiCrAlY was observed to crack and spall early when exposed to the combustion products of dirty fuel-fired burner rigs. This was first indicated in preliminary exposure tests described by Levine and Clark (ref. 11). Samples were exposed to the combustion gases of a Jet A-fired burner rig doped with sodium. Spalling initiated after 40 one hour cycles, and measurable amounts of deposits could be washed from the specimens.

Bratton et al. (ref. 27) describe tests of the early NASA-Lewis coating system and a similar system applied by a commercial vendor. The tests were conducted at Westinghouse as part of a program sponsored by the Electric Power Research Institute (EPRI). A pressurized passage burner rig firing No. 2 diesel fuel was used for this investigation. Impurities in the fuel were 0.24 w/o S, 2 ppm Fe, 0.7 ppm V, 0.3 ppm P, 0.3 ppm Na + K, and other contaminants in the 0.2 to 0.8 ppm range. Various dopants, most frequently Na and V, were added in the 0.5 to 10 ppm range, and in several tests the sulfur level was increased to 0.5 w/o. In some tests additives such as Mg or Cr-Mg-Si were included to determine whether they had any beneficial effect. A Ba additive was present in the as-received fuel for some runs.

Various specimen configurations and test temperatures were employed. Samples were exposed to the combustion gases in cycles lasting 8 to 10 hours, and the maximum total test time per specimen was 131 hours. The coatings remained intact after exposure in only three cases. These were when the fuel was undoped, doped with 1 ppm Na, and doped with 5 ppm Pb. Micrographs showed severe longitudinal cracking after 131 hours in the 1 ppm Na case. For the remaining nine cases the coatings spalled. Usually the failure occurred within the ceramic layer. Complete or nearly complete delamination was only observed in a few cases corresponding to the highest substrate temperatures. Spalling caused by V attack was not controlled by Mg-base additives.

After testing, the surfaces of the specimens used in reference 27 were analyzed by X-ray diffraction analysis and the cross sections were analyzed by electron microprobe analysis. Among the various compositions identified were Na₂SO₄, YPO₄, NaZr₂(PO₄)₃, Mg₃(PO₄)₂, Mg₃(VO₄)₂, MgO, MgSO₄, BaSO₄, Fe₂O₃, and SiO₂. These results helped implicate phosphorous in the undoped fuel as a particularly aggressive contaminant. They also showed that, as expected, Mg-based additives combine with V and P to form refractory compounds. However, apparently enough unreacted V and P remained to react with the coatings.

When Mg was not present, no V-containing compound could be detected by X-ray diffraction analysis. However, vanadium was detected by electron microprobe analysis. Bratton et al., speculated that deposits of V₂O₅(ℓ) may have reacted with the coating to form YVO₄ whose X-ray pattern was masked by YPO₄. Tests by Bratton et al. (ref. 27) and by Zaplatynsky (ref. 28) showed

that V_2O_5 reacts with cubic or tetragonal $ZrO_2-Y_2O_3$. The products are monoclinic ZrO_2 plus a phase identified by Bratton et al. as YPO_4 . Alternatively, they suggest that $V_2O_5(l)$ could have reacted with other contaminants or even the coating to form a glass which would not produce an X-ray pattern.

Hodge et al. (ref. 29) conducted tests at NASA-Lewis which were part of a test program funded by the Department of Energy. An initial series of tests was run on the early Lewis Research Center coating system ZrO_2-12 w/o Y_2O_3 - $NiCrAlY$. The rig used for this study was a Mach 0.3 burner rig fired with Jet A fuel. The level of S in the fuel was about 0.05 w/o. Dopants were added by aspirating aqueous salt solutions into the combustion chamber. The test conditions, specimen temperatures, dopant levels and number of cycles to failure are illustrated in figure 5 of Hodge et al. This figure is presented here as figure 2. The test results generally agree with those from the Westinghouse study. Spalling was observed for every case except the one involving the lower level of Na. However, some erosion of the coating was observed in that case. Photographs of all five specimens and representative micrographs are shown in that report (see figs. 6 and 7, respectively, of Hodge et al.). Those figures are reproduced here as figures 3 and 4. One may note from the specimen photographs that when samples were exposed to V, spalling occurred in the approximate center of the hot zone of the specimen. When exposed to 5 ppm Na, spalling occurred in a cooler region below the hot zone. When exposed to 0.5 ppm Na no failure was observed. When Na plus V were combined, spalling occurred in a region extending from the hot zone to a cooler region above the hot zone. The micrographs show that, as with the Westinghouse investigation, failure occurred within the ceramic layer. With the 2 ppm V case very little ceramic remained attached. This is shown in figure 4(f) and in the unpublished photograph of the adjacent region (P. Hodge, personal communication). With the 0.2 ppm V case and the 5 ppm Na plus 2 ppm V case much of the ceramic remained attached after failure. However, the failed area extended very close to the bond coat in some locations. Examples of this may be seen on the left side of figure 4(b) and the center of figure 4(e). With the 5 ppm Na case, the coating which remains attached after failure is relatively uniform in thickness, and in no location does the failed area approach the bond coat layer (fig. 4(c)).

The observation that failure occurs in the ceramic layer is consistent with the results of Stecura for specimens tested in clean fuel environments. As seen in figure 7 of Stecura (ref. 25) the crack initiates in the ceramic layer parallel to and close to the ceramic/bond coat interface. Levine (ref. 30) tested the tensile strength of $ZrO_2-Y_2O_3/NiCrAlY$ coatings and found that the weakest part of the coating system is in that location.

Palko et al. (ref. 31) tested the early NASA-Lewis coating system in a combination low velocity burner/electric furnace rig. The tests were conducted at General Electric and were part of a program sponsored by the Department of Energy. All of the test specimens were uncooled. They were exposed to the combustion gases of a fuel oil doped with sodium in cycles of about 24 hours. In this study the ceramic coating tended to fail by spalling away completely from the bond coat. Frequently, the substrate was also attacked. Scanning electron microscopy was used to show that $Na_2SO_4(l)$ is adsorbed into the open por-

osity of the coatings. Palko et al. speculate that, upon cooling, differences in thermal expansion between the coating and the solidified salt caused the observed spalling. For most of the experiments, the reported specimen temperature was actually slightly below the melting point of Na_2SO_4 . However, their experimental evidence showed that the salt had been molten. The source of sodium was not specified, but if it had been added as sea salt the Na_2SO_4 deposit could have contained small amounts of K_2SO_4 , Ca_2SO_4 , and MgO (ref. 32). This may have led to a depressed melting point. Alternatively, the actual temperature may have been higher than that recorded by their thermocouple.

D. Preliminary Dirty Fuel Tests of Alternate Coating Systems

These initial results demonstrated that further development was required to tailor thermal barrier coating systems for endurance in dirty environments. A preliminary step towards this goal was taken by Hodge et al. who evaluated 16 coating systems. The test conditions of the 5 ppm Na plus 2 ppm V case described previously were used. In these tests eight specimens were mounted on a rotating multispecimen holder, and the substrate temperature was only measured for the "standard" ZrO_2 -12 w/o Y_2O_3 /NiCrAlY reference sample. Test results are presented in figure 8 of Hodge et al. An abridged version of this figure is presented here as figure 5. According to this figure a ZrO_2 -8 w/o Y_2O_3 /NiCrAlY system lasted more than five times longer than the standard system. Two other coating systems were identified which displayed further improvement in life. One was based on a calcium silicate- $1.8\text{CaO}\cdot\text{SiO}_2$ /NiCrAlY. The other was a cermet 50 v/o MgO -50 v/o NiCrAlY//NiCrAlY. Most of the coatings tested spalled as described above for the standard system. The cermet was an exception. With this coating, continual thinning by microspalling was observed.

Although this investigation was limited in scope, coating systems were identified which had significantly improved durability in the presence of inorganic salt contaminants. Continued research can be expected to provide even greater improvements. Recently, improvements have been made to one of the NASA-Lewis alternate coating systems. The durability of $1.8\text{CaO}\cdot\text{SiO}_2$ was found to be improved when CoCrAlY bond coats are used. This improvement was observed by the author in unpublished cyclic furnace oxidation studies and by Hodge in unpublished Naplus V-doped burner rig tests.

CALCULATION OF CONDENSATE DEW POINT TEMPERATURES AND SPECIMEN TEMPERATURE DISTRIBUTION

Based on the test results described in the previous section it is clear that coating durability is adversely affected by inorganic salt deposits. Insight into the mechanisms for these accelerated failures may be gained by considering the dew points and melting points of the condensates and the temperature distributions within the coatings.

The thermodynamic dew point is the temperature at which a condensate would first appear as a combustion gas is cooled. It is the temperature at which the gas becomes saturated with respect to the partial pressure of the species in

equilibrium with the condensate. Dew points may be calculated if the free energies of formation are available for all of the important components of a chemical system. Kohl and co-workers (refs. 32 to 35) have described how the NASA-Lewis Complex Chemical Equilibrium Computer Program (ref. 36) may be used for these calculations. Recent results have indicated that this type of thermochemical treatment is appropriate for these systems (refs. 32, and 37 to 39). This is because the pertinent chemical reactions apparently are sufficiently rapid for equilibrium to be established.

For the experiments described by Hodge et al., the contaminants of interest are sulfur, sodium, and vanadium. Because the tests had been preliminary in nature, the deposits in the coatings were not intensively analyzed. However, the observed early spalling can be taken as evidence that such deposits were present. The composition of these deposits can be deduced from the analytical results described by Bratton et al. and Palko et al. and from thermodynamic calculations. Condensed phase sodium sulfate, Na_2SO_4 (s or l), is normally expected to form when Na is added to S-containing fuels (e.g., ref. 33). Palko et al. identified deposits of this species from fuels containing Na and S. Bratton et al. detected "significant" quantities of Na_2SO_4 when 5 ppm Na was in the fuel. When only 1 ppm Na was in the fuel Na_2SO_4 could not be identified. When V was the only contaminant added by Bratton et al., vanadium was detected by electron microprobe analysis but not by X-ray diffraction analysis. The author speculated that V_2O_5 deposited and that subsequent reactions prevented detection by X-ray diffraction analysis. The deposits, Na_2SO_4 and V_2O_5 , are also predicted thermodynamically.

When Na and V were the dopants, no phase containing both of these elements was detected (ref. 27). Thermodynamic calculations indicate that the vanadium-containing condensate changes as a function of temperature. At high temperatures the deposit is expected to be $\text{V}_2\text{O}_5(\text{l})$. This is replaced by $\text{Na}_2\text{V}_2\text{O}_6$ at moderate temperatures which is in turn replaced by $\text{V}_2\text{O}_5(\text{s})$ at lower temperatures. Also, at intermediate temperatures Na_2SO_4 may condense. Currently $\text{Na}_2\text{V}_2\text{O}_6(\text{s})$ is the only sodium vanadate considered in the computer analysis. The thermodynamic data for the solid is extrapolated to temperatures above the melting point for the liquid phase. Thus compositions calculated between the melting point and the dew point of $\text{Na}_2\text{V}_2\text{O}_6$ are approximate. Also the activities of the condensates are treated as unity. Nevertheless, these may be considered as "first order calculations" for this system.

Thus, the deposits are Na_2SO_4 when Na and S are present and V_2O_5 when V (and S) are present. Depending on temperature, the deposits are predicted to be Na_2SO_4 , V_2O_5 , and $\text{Na}_2\text{V}_2\text{O}_6$ when Na, V, and S are present. The dew points of these deposits may be calculated for each specific experimental condition using the NASA-Lewis computer program. Actually, a more sophisticated treatment of the deposition process, which allows more accurate dew points and the amount of deposit to be calculated, has been described by Rosner, Kohl, and co-workers (ref. 32). This also is a treatment which is, in part, thermodynamic and makes use of the NASA-Lewis computer program. Mass transport across the boundary layer formed around the test specimen is also considered. This treatment was applied in reference 32 to Na_2SO_4 deposited from the same

type of burner rig flames as were used by Hodge et al. For that case there was very little difference between the thermodynamic dew points and the more refined condensation onset temperatures. The calculated values also agreed very well with the experimentally determined dew points.

No consideration was given to the possible effects of condensation in the interconnected pores and microcracks of the coating. Curvature at the base of a crack or in a very small pore could be high enough to support the liquid phase at temperatures above the thermodynamic dew point. Such effects would be small, assuming that the total volume of appropriate locations is small. This phenomena may deserve further attention, however it is not expected to affect the interpretation of the experiments analyzed in this paper.

For the case of thermal barrier coatings exposed to doped combustion gases (ref. 29), the thermodynamic dew points were calculated to the nearest 5° C for the conditions of the five experiments of interest. They are presented in table 1. Also, the number of cycles to failure, the melting points of the condensates, and experimental observations are given for reference. The temperatures at the leading edge of the test specimen were measured optically at the surface and by a thermocouple in the center of the hot zone in the substrate. The temperature drop ΔT within both the thermal barrier coating, TBC, and the bond coat, BC, are related by a one-dimensional energy balance (ref. 40).

$$\left(\frac{K \Delta T}{d}\right)_{BC} = \left(\frac{K \Delta T}{d}\right)_{TBC}$$

Here, K is the thermal conductivity and d is the coating thickness. The ratio K_{BC}/K_{TBC} was taken to be 17 (ref. 40). The measured value of d_{TBC} is 0.038 cm and that of d_{BC} is 0.013 cm. The substrate thermocouple was located 0.048 cm below the substrate-bond coat interface, and it was covered with a nickel-base alloy braze. The temperature drops were calculated from the measured ΔT between the surface and the substrate and the above expression. The thermal conductivities of the braze and bond coat were assumed to be equal, as a first approximation, and d_{BC} was taken initially as the sum of the bond coat thickness plus the additional distance to the thermocouple. The temperature at the substrate/bond coat interface was then obtained by linear interpolation of the temperatures in the metal layers. This gives a calculated temperature drop of about 130° C across the ceramic and 3° C across the bond coat. The calculated ceramic/bond coat interface temperature was therefore 852° C, and the calculated bond coat/ substrate temperature was 849° C. Because the temperature drop within the metal is small, any error resulting from the assumption that K_{BRAZE} equals K_{BC} is minimal.

At the ends of the specimens the surface temperatures were measured to be about 890° C (P. Hodge, personal communication). Assuming, as an approximation, the same temperature drops across the ceramic at the ends as at the center, the lowest leading edge substrate temperature was about 760° C.

ANALYSIS OF THE EFFECTS OF SALT DEPOSITION ON THE
DURABILITY OF THERMAL BARRIER COATINGS

The failure characteristics of the specimens may now be discussed in terms of the dew point/melting point and coating temperatures described in the previous section. For the first case in table 1, 5 ppm Na, the dew point of the Na_2SO_4 condensate is less than the surface temperature at the hot zone of the specimen. Thus, if Na_2SO_4 were to deposit, its vapor precursors would first have to penetrate through a portion of the coating. This should significantly reduce the deposition rate. In fact, based on the location of the spalled area, figure 3(c), Na_2SO_4 appears to have preferentially deposited in cooler regions outside of the hot zone. At this location the surface temperature was low enough to permit deposition. Once the $\text{Na}_2\text{SO}_4(\ell)$ deposited it would diffuse or "wick" through the open porosity of the coating (ref. 31). However, these processes would cease at any point where the temperature in the coating was less than 884°C , the melting point of sodium sulfate. Even in the hot zone the temperature at the bond coat/ceramic interface is only 855°C . Thus, Na_2SO_4 should not penetrate all the way to the bond coat and no high temperature corrosion of the bond coat or substrate should occur.

The processes described above are illustrated schematically in figure 6. The dew point and melting point for Na_2SO_4 in this case are plotted on the right side of the figure. The temperatures for the condensates in the other four experiments of interest are also given. The estimated gas, boundary layer, and specimen temperatures are plotted in the remainder of the figure. This figure illustrates that the surface temperature is equal to the dew point temperature at a location which is intermediate between the center, or hot zone, and the ends of the specimen. The deposit at this point can penetrate into the coating until the depth is reached where the coating temperature drops below the melting point of the deposit. The estimated perpendicular depth of penetration is given by the two vertical, dashed lines. Because figure 6 must be considered to be very approximate, the depth of penetration can not be quantitatively compared with the actual failure location (figs. 3(c) and 4(c)). However, it is qualitatively correct and shows why failure occurred in the ceramic outside of the hot zone and well above the bond coat.

Because Na_2SO_4 does not react with the ceramic under the conditions of these experiments (refs. 27, 28, 31, and 41), its effects must be mechanical. The $\text{Na}_2\text{SO}_4(\ell)$ would enter the pores and microcracks of the ceramic coating and solidify upon cooling. Palko, et al., suggest that differences in thermal expansion between the salt and the ceramic may cause the failure. An even simpler mechanism is possible. By filling or internally coating the pores with Na_2SO_4 , the coating density may effectively increase to a level above that required for the ceramic to retain its ability to accommodate cyclic thermal stresses. This critical level is given in reference 23 as 88% of theoretical density. As described earlier cracking parallel to the substrate is observed even when clean fuels are used. When salts are present the effects leading to the cracking would be magnified. The result is the observed early spalling.

The layer of coating which remained after spalling would provide less thermal protection to the underlying substrate. Presumably if the remaining ceramic

were thin enough the temperature of the underlying metal could exceed the melting point of Na_2SO_4 . High temperature corrosion would then be possible at this location. Claus et al. (ref. 42), have shown that if the spalled area is not too large the substrate in the spalled area may be cooled by conduction to the surrounding substrate. Under these conditions the spalled coating could remain protective against high temperature corrosion.

For the second case in table 1, 0.5 ppm Na, the dew point temperature of Na_2SO_4 is less than the temperature at the substrate/bond coat interface in the hot zone and less than the surface temperature over the entire specimen. Therefore, Na_2SO_4 should not condense. Furthermore, the dew point is below the melting point so that even if Na_2SO_4 could condense it would only do so as a solid. It would not diffuse or "wick" throughout the coating and could even tend to seal the coating. Therefore, long lives were observed because this test was no more severe than an oxidation test (fig. 3(d)).

For the third and fourth case in the table 2, 2 ppm V and 0.2 ppm V respectively, $\text{V}_2\text{O}_5(\ell)$ is expected to have been the deposit on the surface of the sample. Because its melting point is low, $\text{V}_2\text{O}_5(\ell)$ could permeate the entire coating. For the high vanadium case this apparently led to the observed spalling very close to the bond coat interface (fig. 4(f)). The failure was not as close to the interface in the low vanadium case (ref. 4(f)). For both cases failure occurred in the hot zone of the test specimen (figs. 3(e) to (f)).

The deposits of V_2O_5 can react with the coating and failure would occur by a combination of chemical and mechanical modes. If, as described earlier, the V_2O_5 caused a significant amount of the zirconia to convert to the monoclinic form, the coating would become mechanically unstable towards thermal cycling. Monoclinic zirconia undergoes a significant volume change due to its conversion to a tetragonal phase of lower thermal expansion. The filling or internal coating of the porosity could enhance this instability. The differences in test lives between the third and fourth cases appears to have been due directly to the difference in vanadium concentration. A tenfold increase in vanadium concentration caused the test life to decrease by a factor of eight. If the duration of the test had been longer, bond coat or substrate attack should also have been possible.

For the fifth case, 5 ppm Na plus 2 ppm V, $\text{Na}_2\text{V}_2\text{O}_6(\ell)$ would probably be the condensate. It would deposit over the entire surface of the coating and could penetrate throughout the entire coating. A more intensive investigation of the deposit or a more accurate calculation would be required to ensure that no mixed $\text{V}_2\text{O}_5 - \text{Na}_2\text{V}_2\text{O}_6$ phases were present. Even if this were the case any conclusions concerning this experiment should not be greatly altered. In the cooler regions above and below the hot zone $\text{Na}_2\text{SO}_4(\ell)$ also could condense. Failure occurred in this case within the coating in a manner similar to what was observed in the 0.5 ppm V case. It is interesting to note that in this combined Na plus V case spalling occurred both in and above the hot zone (fig. 3(b)). This could have been due to the effects of $\text{Na}_2\text{V}_2\text{O}_6$ in the hot zone and the combined effects of $\text{Na}_2\text{V}_2\text{O}_6$ plus Na_2SO_4 above the hot zone. The coating lasted longer in the presence of $\text{Na}_2\text{V}_2\text{O}_6$ than in the presence

of V_2O_5 . This probably results from V_2O_5 being more reactive than $Na_2V_2O_6$.

The above discussion applies in general to the tests at GE (ref. 31) and Westinghouse (ref. 27). At GE the uncooled samples were exposed to Na_2SO_4 deposits at temperatures apparently always above the melting point and below the dew point. Sodium sulfate deposited on the samples and permeated through the entire coating system. This led to spalling at the ceramic/bond coat interface and hot corrosion attack of the substrate.

For the experiments conducted at Westinghouse, the test specimens were always exposed to multiple contaminants from the No. 2 diesel fuel plus dopants and additives. A quantitative assessment of the results for each condition studied would be rather laborious and beyond the scope of the current discussion. Many of the cases were similar to the experiments of Hodge et al., when the contaminants were Na plus V. That is, conditions can be expected to have been severe due to high dew points, low melting points, and reactivity towards the coating. Usually spalling occurred within the coating as described by Hodge et al. for Na plus V. At the highest temperatures the coating failed at the bond coat interface and metal attack was observed. This was probably caused by higher reaction rates at elevated temperatures.

An especially important observation of Bratton et al. was that Mg-based additives in quantities equivalent to three times the weight of V in the fuel did not control attack by P and V. This was a case where even though the majority of the deposits were solids there was still apparently enough V- and P-containing liquid phases remaining to permeate and attack the coating.

SUMMARY OF RESULTS

This paper reviews previous tests of a NASA-Lewis thermal barrier coating system exposed to the combustion gases of dirty fuel fired burner rigs at Westinghouse, GE, and NASA-Lewis. For the NASA tests, the dew points of the predicted condensates were calculated for the test conditions employed. These dew points and the melting points of the condensates were then related to the observed failure modes of the coated test specimens.

The coatings tested at NASA-Lewis (ref. 29) were formed from a 0.038 cm layer of ZrO_2 -12 w/o Y_2O_3 over a 0.013 layer of NiCrAlY bond coat. Test temperatures in the hot zone of the test specimen were 982° C at the surface and 852° C at the ceramic/ bond coat interface. The coatings were exposed to combustion gases doped to two levels of sodium (0.5 and 5 ppm with respect to the fuel), two levels of vanadium (0.2 and 2 ppm), and one level of sodium plus vanadium (2 ppm V, 5 ppm Na). Dew points were calculated for the predicted condensates in each specific case. These were used along with condensate melting points to explain observed specimen failure locations. Several observations could be made based on dew point/melting point considerations and the referenced test conditions:

(1) The most severe condition to which the coatings could be exposed are expected to be those cases when the melting point of the condensate is less

than the bond coat temperature while the dew point of the condensate exceeds the specimen temperature. Under these conditions the liquid condensate can be expected to deposit on the coating surface and to penetrate throughout the entire coating system. This condition was met when the condensate was $V_2O_5(l)$ formed when vanadium (0.2 to 2 ppm) was added to the combustion gas as well as when the condensate was $Na_2V_2O_6(l)$ formed when Na plus V (5 ppm Na, 2 ppm V) were added. As described by Hodge et al. (ref. 29), when the coating was exposed to such conditions it failed early and failure occurred in the ceramic very close to the bond coat/ceramic interface. This region is essentially the same location where cracks were observed by Stecura (ref. 25) in coatings exposed to clean fuels. (Of course in those tests no salt contaminants were present so much longer test lives were observed.) This location of the failure can be considered to correspond to the weakest location in the coating system.

(2) There are two conditions for which dopants were not expected to lead to coating failure. One was when the dew point was less than the surface temperature. The other was when the dew point was less than the melting point. Experimentally, when the dew point was less than the surface temperature there apparently was little penetration of the coating even though the coating was permeable. When the dew point was less than the melting point of the condensate the salt would have deposited only as a solid. Such a solid would not be expected to harm the coating because of its limited mobility. Both of these conditions were met when the lower level of sodium was added to the combustion gases. Again, the dew point/melting point approach appears valid because, experimentally, no failures were observed under the above conditions. Thus, this test was probably no more severe than an oxidation test.

(3) When high levels of sodium were present the dew point of the Na_2SO_4 condensate was less than the surface temperature in the hot zone. In cooler regions the dew point exceeded the surface temperature. Experimentally, no failure occurred in the hot zone. However, failure was observed to shift to a cooler region on the test specimen. In these cooler regions, where the melting point of the condensate was less than the surface temperature but higher than the bond coat temperature, the condensate could be expected to penetrate part way into the ceramic coating. One would expect that the coating would fail well within its own thickness. Again, experimentally, this was observed in the high sodium case.

REFERENCES

1. Grisaffe, S. J.; Levine, S. R.; and Clark, J. S.: Thermal Barrier Coatings. NASA TM-78848, 1978.
2. Aviation Turbine Fuels Am. Natl. Stand. Inst./Am. Soc. Test. Mater. Stand. D1655-78, 1978.
3. Duncan, R. L.; and Dolbec, A. C.: A Program to Improve Gas Turbine Availability and Reliability. Turbomachinery International, March, 1979, pp. 46-51.

4. Freche, J. C.; and Ault, G. M.: Progress in Advanced High Temperature Turbine Materials, Coatings, and Technology. NASA TM X-73628, 1977.
5. Grisaffe, S. J.: Coatings and Protection. The Superalloys, C. Sims and W. C. Hagel, eds., John Wiley and Sons, Inc., 1972, Chapter 12, pp. 341-370.
6. Chatterji, D., Devries, R. C.; and Romeo, G.: Protection of Superalloys for Turbine Application. Advances in Corrosion Science and Technology, Vol. 6, M. G. Fontana and R. W. Staehle, eds., Plenum Press, 1976, pp. 1-87.
7. Goward, G. W.: Protective Coatings for High Temperature Alloys - State of Technology. Symposium on Properties of High Temperature Alloys, Z. A. Foroulis, and F. S. Pettit, eds., The Electrochemical Society, Inc., 1976, pp. 806-823.
8. Clark, J. S.; Nainiger, J. J.; and Hyland, R. E.: Potential Benefits of a Ceramic Thermal Barrier Coating on Large Power Generation Gas Turbines. NASA TM-73712, 1977.
9. Ingham, H. S., and Shepard, G. P.: Flame Sprayed Handbook. Vol. III, Plasma Flame Process. Metco Inc., 1965.
10. Grisaffe, S. J.: A Simplified Guide to Thermal Spray Coatings. Mach. Des., vol. 39, no. 17, July 20, 1967, pp. 174-181.
11. Levine, S. R., and Clark, J. S.: Thermal Barrier Coatings - A Near Term, High Payoff Technology. NASA TM X-73586, 1977.
12. Stepka, F. S.; and Liebert, C. H.; and Stecura, S.: Summary of NASA Research on Thermal Barrier Coatings. NASA TM X-73584, 1977.
13. Schafer, L. J., Jr.: Comparison of Theoretically and Experimentally Determined Effects of Oxide Coatings Supplied by Fuel Additives on Uncooled Turbine-Blade Temperature During Transient Turbojet-Engine Operation. NACA RM E53A19, 1953.
14. Bartoo, E. R., and Clure, J. L.: Experimental Investigation of Air-Cooled Turbine Blades in Turbojet Engine XIII - Endurance Evaluation of Several Protective Coatings Applied to Turbine Blades of Nonstrategic Steels. NASA RM E53E18, 1953.
15. Hjelm, Lawrence N.; and Bornhorst, Bernard R.: Development of Improved Ceramic Coatings to Increase the Life of XLR 99 Thrust Chamber. Research-Airplane-Committee Report on Conference on the Progress of the X-15 Project. NASA TM X-57072, 1961, pp. 227-253.
16. Curren, Arthur N.; Grisaffe, Salvatore J.; and Wycoff, Kurt C.: Hydrogen Plasma Tests of Some Insulating Coating Systems for the Nuclear Rocket Thrust Chamber. NASA TM X-2461, 1972.

17. Liebert, C. H., and Stecura, S.: Ceramic Thermal Protective Coating Withstands Hostile Environment of Rotating Turbine Blades. NASA Tech Brief B75-10290, 1975.
18. Stecura, S.: Two-Layer Thermal Barrier Coating for Turbine Airfoils - Furnace and Burner Rig Test Results. NASA TM X-3425, 1976.
19. Stecura, S.; and Liebert, C. H.: Thermal Barrier Coating System. U.S. Patent 4,055,705, Oct. 25, 1977.
20. Stecura, S.: Two-Layer Thermal Barrier Coating for High Temperature Components. Am. Ceram. Soc. Bull., vol. 56, no. 12, Dec. 1977, pp. 1082-1089.
21. Nijpjes, N. M.: ZrO₂-Coatings on Nimonic Alloys. Sixth Plansee Seminar on High Temperature Materials, F. Benesovsky, ed., Springer-Verlag, 1969, pp. 481-499.
22. Cavanagh, J. R., et al.: The Graded Thermal Barrier - A New Approach for Turbine Engine Cooling. AIAA Paper 72-361, Apr. 1972.
23. Tucker, R. C., Jr.; Taylor, T. A.; and Weatherly, M. H.: Plasma Deposited MCrAlY Airfoil and Zirconia/MCrAlY Thermal Barrier Coatings. Presented at the 3rd Conference on Gas Turbine Materials in a Marine Environment. (Univ. Bath, Bath, England), Sep. 20-23, 1976, Session VII, Paper 2.
24. Gaffin, W. O., and Webb, D. E.: JT8D and JT9D Jet Engine Performance Improvement Program - Task 1, Feasibility Analysis. (PWA-5518-38, Pratt and Whitney Aircraft Group; NASA Contract NAS3-20630.) NASA CR-159449, 1979.
25. Stecura, S.: Effects of Compositional Changes on the Performance of a Thermal Barrier Coating System. NASA TM-78976, 1978.
26. Scott, H. G.: Phase Relationships in the Zirconia-Yttria System. J. Mater. Sci., vol. 10, no. 9, Sep. 1975, pp. 1527-1535.
27. Bratton, R. J.; Singhal, S. C.; and Lee, S. Y.: Ceramic Turbine Components Research and Development, Part II - Evaluation of MCrAlY/ZrO₂ (Y₂O₃) Thermal Barrier Coatings Exposed to Simulated Turbine Environments. Final Report Summary, Westinghouse R&D Center, 1979. Also, Bratton, R. J.; Singhal, S. C.; and Hays, W.: Ceramic Rotor Blade Development - Part I. Ceramic Thermal Barrier Coatings. Semi-Annual Tech. Rep. -4, Westinghouse R&D Center, 1977.
28. Zaplatynsky, I.: Reactions of Yttria-Stabilized Zirconia with Oxides and Sulfates of Various Elements. DOE/NASA/2593-78/1, NASA TM-78942, 1978.
29. Hodge, P. E., et al.: Thermal Barrier Coatings. Burner Rig Hot Corrosion Test Results. DOE/NASA/2593-78/3, NASA TM-79005, 1978.
30. Levine, S. R.: Adhesive/Cohesive Strength of a ZrO₂-12 w/o Y₂O₃/NiCrAlY Thermal Barrier Coating. NASA TM-73792, 1978.

31. Palko, J. E.; Luthra, K. L.; and McKee, D. W.: Evaluation of Performance of Thermal Barrier Coatings Under Simulated Industrial/Utility Gas Turbine Conditions. Final Report, General Electric Co., 1978.
32. Kohl, F. J.; et al.: Theoretical and Experimental Studies of the Deposition of Na_2SO_4 from seeded Combustion Gases. J. Electrochem. Soc., vol. 126, no. 6, 1979, 1054-1061; also NASA TM X-73683, 1977.
33. Kohl, F. J.; Stearns, C. A.; and Fryburg, G. C.: Sodium Sulfate: Vaporization Thermodynamics and Role in Corrosion Flames. International Symposium on Metal-Slag-Gas Reactions and Processes by Z. A. Foroulis and W. W. Smeltzer, eds., The Electrochemical Soc., 1975, pp. 649-664; also NASA TM X-71641, 1975.
34. Bennett, J. E.; et al.: Preliminary Evaluation of the Role of K_2S in MHD Hot Stream Seed Recovery. DOE/NASA/2674-79/1, NASA TM-79114, 1979.
35. Deadmore, D. L.; Lowell, C. E.; and Kohl, F. J.: The Effect of Fuel-to-Air Ratio on Burner-Rig Hot Corrosion. NASA TM-78960, 1978.
36. Gordon, S.; and McBride, B. J.: Computer Program for Calculation of Complex Chemical Equilibrium Compositions Rocket Performance, Incident and Reflected Shocks, and Chapman-Jouget Detonations. NASA SP-273, 1976, Revised.
37. Stearns, C. A., et al.: Investigation of Gaseous Sodium Sulfate In a Doped Methane-Oxygen Flame. J. Electrochem. Soc., vol. 124, no. 12, 1977, pp. 1145-1146; also NASA TM X-73600, 1977.
38. Fryburg, G. C.; et al.: Formation of Na_2SO_4 and K_2SO_4 in Flames Doped with Sulfur and Alkali Chlorides and Carbonates. NASA TM-73794, 1977.
39. Deadmore, D.; and Lowell, C.: Burner Rig Alkali Salt Corrosion of Several High Temperature Alloys. NASA TM X-73659, 1977.
40. Liebert, C. H.; and Stepka, F. S.: Potential Use of Ceramic Coating as a Thermal Insulation on Cooled Turbine Hardware. NASA TM X-3352, 1976.
41. Dapkunas, S. J.; and Clarke, R. L.: Evaluation of the Hot-Corrosion Behavior of Thermal Barrier Coatings. NSRDC-4428, Naval Ship Research and Development Center, 1974. (AD-A000093)
42. Claus, R. W.; Wear, J. D.; and Liebert, C. H.: Ceramic Coating Effect on Liner Metal Temperatures of Film-Cooled Annular Combustors. NASA TP-1323, 1979.

TABLE 1. - CALCULATED DEW POINT TEMPERATURES FOR CONDENSATES AND EXPERIMENTAL OBSERVATIONS IN EXPERIMENTS OF HODGE ET AL. (REF. 29)

Dopant level (referred to fuel)	Predicted condensate	Dew point temperature, T_{dp} ($^{\circ}$ C)	Melting point temperature, T_{mp} ($^{\circ}$ C)	Cycles to coating failure for ZrO_2-12 w/o Y_2O_3 / NiCrAlY	Footnote
5 ppm Na	Na_2SO_4 (l)	920	884	92	A,B
0.5 ppm Na	Na_2SO_4 (s)	845	884	>1300	A,C
2 ppm V	V_2O_5 (l)	1210	670	25	A,D
0.2 ppm V	V_2O_5 (l)	1125	670	200	A,E
5 ppm Na + 2 ppm V	V_2O_5 (l)	1210	670	43	A,F,G
	$Na_2V_2O_6$ (l)	~1155	627		
	Na_2SO_4 (l)	~910	884		
	V_2O_5 (s)	575	670		

- A. Mach 0.3 burner rig, fuel/air ratio 0.042; specimen temperatures: 982° C surface (T_{surf}), 852° C bond coat/ceramic interface (T_{bc}) in the hot zone; 890° C surface, 760° C bond coat/ceramic interface at tip and root of test specimen.
- B. $T_{bc} < T_{mp} < T_{dp} < T_{surf}$. No failure of ceramic in hot zone. Failure outside of hot zone well above bond coat.
- C. $T_{dp} < T_{bc} < T_{mp} < T_{surf}$. No failure of ceramic.
- D. $T_{mp} < T_{bc} < T_{surf} < T_{dp}$. Failure of ceramic in hot zone very close to bond coat.
- E. $T_{mp} < T_{bc} < T_{surf} < T_{dp}$. Failure of ceramic in hot zone relatively close to bond coat.
- F. Only one V-containing condensed phase is stable in each temperature range. $Na_2V_2O_6$ is stable at specimen temperatures.
- G. $T_{mp} < T_{bc} < T_{surf} < T_{dp}$ for $Na_2V_2O_6$. $T_{bc} < T_{mp} < T_{dp} < T_{surf}$ for Na_2SO_4 . Failure of ceramic in and outside of hot zone relatively close to bond coat.

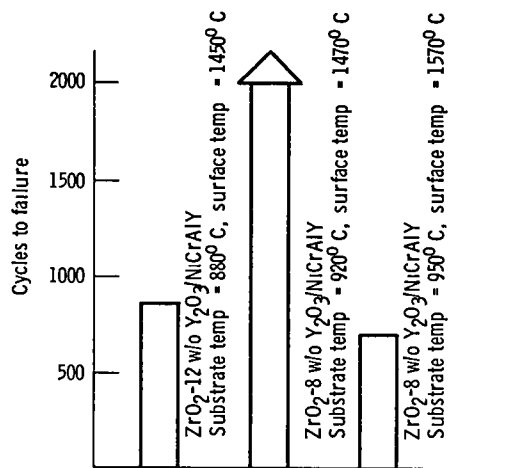


Figure 1. - Mach 1 burner rig test results of two ZrO₂-Y₂O₃/NiCrAlY thermal barrier coating systems (ref 25) (The arrow indicates that the test was stopped before the specimen failed)

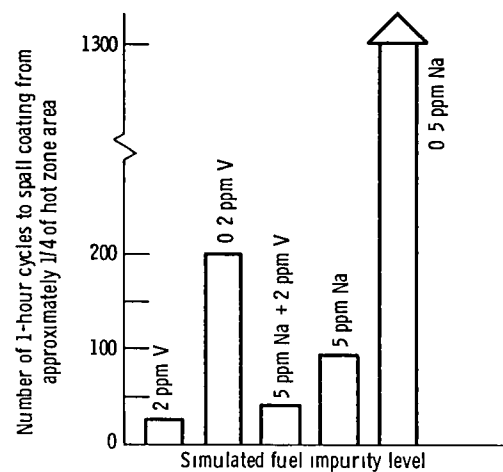
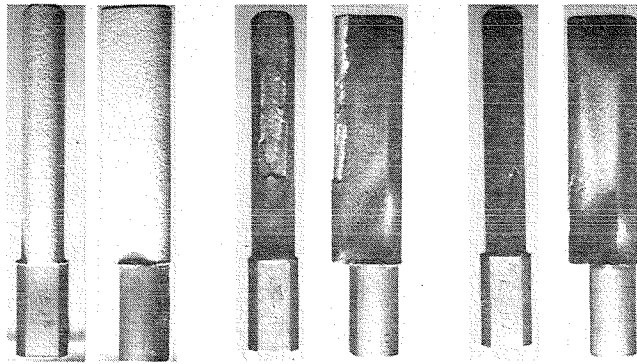


Figure 2. - Single specimen Mach 0.3 burner rig fuel impurity sensitivity tests of ZrO₂-12 w/o Y₂O₃/NiCrAlY thermal barrier coating system (ref 29) Operating conditions metal substrate temperature, 843° C, ceramic surface temperature, 982° C

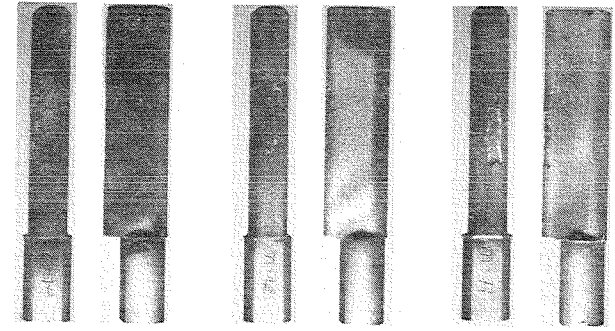


(a) As sprayed ZrO_2-12 w/o Y_2O_3 NiCrAlY.

(b) 43 1-Hour cycles, 5 ppm Na + 2 ppm V.

(c) 92 1-Hour cycles, 5 ppm Na.

CS-79-518



(d) 1300 1-Hour cycles, 0.5 ppm Na.

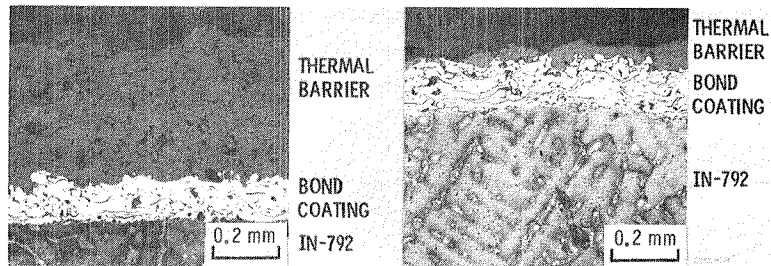
(e) 200 1-Hour cycles, 0.2 ppm V.

(f) 25 1-Hour cycles, 2 ppm V.

Figure 3. - Concluded.

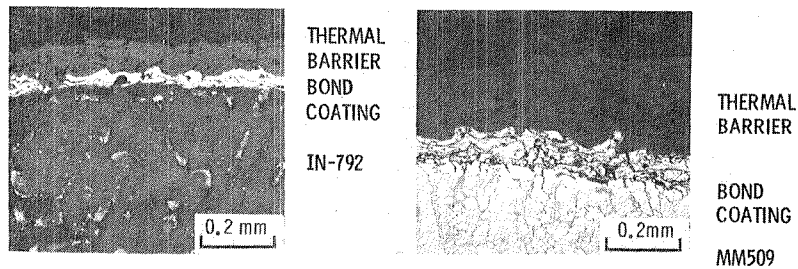
CS-79-523

Figure 3. - Typical photographs of single specimen thermal barrier coated IN-792 and MM509 hollow erosion bars after exposure to Mach 0.3 combustion gases doped with fuel equivalent amounts of Na and V (ref. 29). Time to spall approximately 1/4 hot zone area is indicated. Operating conditions: $982^{\circ}C$ ceramic surface temperature; and $843^{\circ}C$ substrate metal temperature.



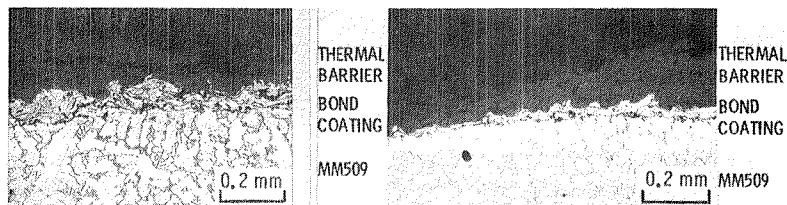
(a) As sprayed ZrO_2 -12 w/o Y_2O_3 / NiCrAlY. CS-79-517 (b) 43 1-Hour cycles, 5 ppm Na + 2 ppm V.

Figure 4. - Representative microstructures of hot zones of ZrO_2 -12 w/o Y_2O_3 / NiCrAlY-coated IN-792 and MM509 hollow erosion bars after exposure to Mach 0.3 combustion gases doped with fuel equivalent amounts of Na and V. Time to spall approximately 1/4 of hot zone area is indicated. Operating conditions: 982° C ceramic surface temperature; 843° C metal substrate temperature.



(c) 92 1-Hour cycles, 5 ppm Na. CS-79-519 (d) 1300 1-Hour cycles, 0.5 ppm Na.

Figure 4. - Continued.



(e) 200 1-Hour cycles, 0.2 ppm V.

(f) 25 1-Hour cycles, 2 ppm V.

Figure 4. - Concluded.

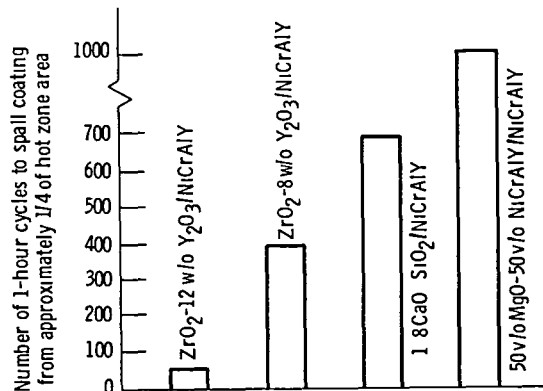


Figure 5 Multiple specimen Mach 0.3 burner rig test of thermal barrier coating systems on IN-792 cooled hollow erosion bars (ref. 29). Standard coating system and three improved compositions. Operating conditions: fuel impurity equivalent of 5 ppm Na + 2 ppm V, metal substrate temperature, 843° C, ceramic surface temperature, 982° C.

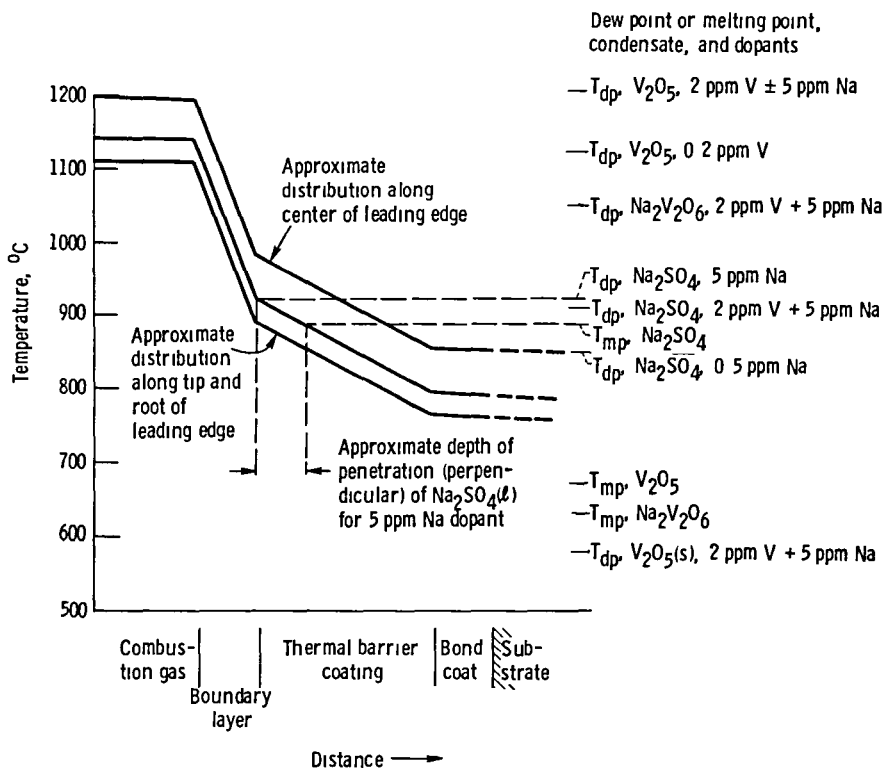


Figure 6 - Relationship between estimated temperature distributions across thermal barrier coating systems and the melting point/dew points of combustion gas condensates

1 Report No NASA TM-79205	2 Government Accession No	3 Recipient's Catalog No	
4 Title and Subtitle ANALYSIS OF THE RESPONSE OF A THERMAL BARRIER COATING TO SODIUM- AND VANADIUM-DOPED COMBUSTION GASES		5 Report Date	
		6 Performing Organization Code	
7 Author(s) Robert A. Miller		8 Performing Organization Report No E-090	
		10 Work Unit No	
9 Performing Organization Name and Address National Aeronautics and Space Administration Lewis Research Center Cleveland, Ohio 44135		11 Contract or Grant No	
		13 Type of Report and Period Covered Technical Memorandum	
12 Sponsoring Agency Name and Address U.S Department of Energy Fossil Fuel Utilization Division Washington, D C 20545		14 Sponsoring Agency-Code Report No DOE/NASA/2593-79/7	
		15 Supplementary Notes Prepared under Interagency Agreement EF-77-A-01-2593 Prepared for Eighth Midwest High Temperature Chemistry Conference, Milwaukee, Wisconsin, June 4-6, 1979	
16 Abstract Published data on the behavior of zirconia-based thermal barrier coatings exposed to combustion gases doped with sodium and vanadium were analyzed with respect to calculated condensate dew points and melting points. Coating temperatures, failure locations, and depths were reasonably well correlated.			
17 Key Words (Suggested by Author(s)) Calcium silicates; Ceramic coatings; Deposits; Gas turbine engines; Thermodynamic properties; Zirconium oxides; Thermal protection; Thermal stresses		18 Distribution Statement Unclassified - unlimited STAR Category 26 DOE Category UC-25	
19 Security Classif (of this report) Unclassified	20 Security Classif (of this page) Unclassified	21 No of Pages	22 Price*

End of Document